COMPLEMENTARY COMPLEX-VALUED SPECTRUM FOR REAL-VALUED DATA: REAL TIME ESTIMATION OF THE PANORAMA THROUGH CIRCULARITY-PRESERVING DFT

Bruno Scalzo Dees[1], *Scott C. Douglas*[2], *Danilo P. Mandic*[1]

[1] Department of EEE, Imperial College London, London, SW7 2BT, UK
[2] Department of EE, Southern Methodist University, Dallas, Texas 75275, US
Emails: {bs1912, d.mandic}@imperial.ac.uk, douglas@lyle.smu.edu

ABSTRACT

This work sheds a new light on the spectral whitening effects of the sliding discrete Fourier transform (DFT) and uses it as a basis for a novel technique for circularity-preserving spectral estimation. This makes it possible to utilise full available spectral information, unlike the existing methods which ignore the phase spectrum. We then use the so introduced circularity-preserving DFT to show that the Wiener filter can be used to estimate the recently introduced second-order complementary spectral measure, termed the panorama, even in the critical cases of short data windows and incoherent sampling. Numerical examples demonstrate the ability of the proposed procedure to estimate the spectral circularity and the panorama, even in a streaming-data setting for which the current methods are inadequate.

Index Terms— complex circularity, panorama, sliding DFT, spectral noncircularity, Wiener filtering.

1. INTRODUCTION

Spectral analysis techniques for real-valued signals typically operate in the complex-valued frequency domain based on magnitude-only models, thus not accounting for the phase information [1]. In other words, conventional spectral estimation makes a fundamental assumption that the phase of these complex representations is uniform and thus not informative. Such an assumption implies that the probability density function (pdf) of an observed complex random variable is *circular*, or *rotation-invariant*, in the complex plane [2].

It has now been widely accepted that for a complete statistical description of complex random variables, we need to employ the so-called augmented complex statistics which, for a complex-valued random variable $\mathbf{x} \in \mathbb{C}^N$, incorporates both the standard covariance, $\mathbf{R} = E\{\mathbf{x}\mathbf{x}^H\}$, and another second-order moment, the pseudo-covariance, $\mathbf{P} = E\{\mathbf{x}\mathbf{x}^T\}$ [3, 4]. Therefore, as with general complex random variables, the Fourier coefficient $X[m]$ at a frequency m has two distinctive second-order statistics: (i) the real-valued Hermitian variance $E\{X[m]X^*[m]\} = E\{|X[m]|^2\}$, also known as the power spectrum; (ii) the lesser-known, complex complementary variance $E\{X^2[m]\}$, also termed the spectral pseudo-variance or the *panorama* [5]. If the panorama is equal to zero, then the random variable $X[m]$ is said to be *proper* [3], or *second-order circular* [6]. Otherwise, for *improper* or *second-order noncircular* random variables the panorama does not vanish. This implies a rotation-dependent probability distribution which manifests itself in unequal powers or degree of correlation between the real and imaginary part of $X[m]$. Unlike the time domain, the second-order noncircularity (impropriety) in the spectral domain has received comparatively little coverage, yet it offers much scope and additional degrees of freedom for enhanced estimation [5, 7].

It was first noted in [6] that wide-sense stationary (WSS) random signals have circular Fourier components, whereas deterministic signals yield highly noncircular Fourier components; the evidence that real-valued nonstationary random signals are second-order noncircular (or improper) was presented in [8]. Spectral noncircularity in complex-valued speech spectra was observed in [9, 10], and has been related to the modulation frequency content [11, 12], while the effectiveness of spectral noncircularity for detection of speech was empirically demonstrated in [13, 14, 15].

Going back to the rotation-dependence of the pdf, impropriety is strongly related to the phase characteristics of a signal in the time and frequency domains. Indeed, the complementary variance, $E\{X^2[m]\}$, parametrizes the eccentricity and angle of an elliptical probability distribution in the complex plane [16], which suggests that impropriety in the frequency domain corresponds to a deterministic-like, relative timing of harmonic components in the time domain. In this way, phase information becomes indispensable in the analysis of approximately periodic signals [11].

This all suggests the importance of designing novel estimators of spectral circularity, especially given that the existing solutions are scattered across several areas of engineering. The *panorama* was formally introduced in [5], defined as the Fourier transform of a zero-mean autoconvolution estimated using ensemble averaging. In conjunction with the conventional power spectrum, that is, the Fourier transform of the zero-mean autocorrelation, a detector for deterministic sinusoidal components in the presence of Gaussian noise was proposed. On the other hand, computing the panorama from a single realization would simply estimate the power spectrum, as it is maximally noncircular. To overcome this issue, the same authors introduced a technique for estimating the absolute value of the panorama of a single-channel signal [7], using block processing based on time-domain averages of the DFT. Subsequently, estimators of spectral circularity were proposed in [17, 2].

There remain several issues that need to be addressed prior to a more widespread application of spectral circularity, these include:

1. Current methods estimate the absolute value of the spectral circularity quotient, as opposed to its inherent complex value, which is essential to maintaining the phase information [4, 5, 7].
2. Existing methods for single-channel panorama estimation are block-based and their performances are highly dependent on the window length and window function. Indeed, non-rectangular window functions may be detrimental to the performance as the autoconvolution vector contains the most recent information at its right-hand end, which is suppressed by most window functions.
3. The effect of *incoherent sampling* on the circularity of the Fourier coefficients was discussed in [15], however no rigorous solution is provided to counteract this effect.

In this work, we extend the work in [5, 15, 7] to address the above caveats encountered when estimating spectral circularity and the panorama using the sliding DFT. This is achieved by first revisiting the spectral whitening property of the sliding DFT in order to exploit the effects of the sliding *phase frame of reference* and *incoherent sampling*. Next, the circularity-preserving DFT is proposed as a key tool for reliable single-realisation estimation of the panorama, and its relation to spectral circularity is highlighted. Finally, an adaptive method for single-realisation panorama estimation is proposed and its usefulness is demonstrated over an example in harmonic analysis.

2. SPECTRAL CIRCULARITY ESTIMATION

2.1. Spectral whitening of the DFT

We next show that the well-known whitening effect of the sliding DFT arises from a phase-spectrum shift which is inherent between every two discrete time increments, n and $(n+1)$. This, in turn, causes deterministic phase progressions, $e^{\jmath\omega_m}$, which destroy the alignment of complex-valued samples in time within each frequency bin [2]. To address the causes of this phase progression, consider a sliding segment of a real-valued signal at time instant n, $\mathbf{x}_n = [x_n, ..., x_{n+N-1}]^T \in \mathbb{R}^N$, the DFT of which is defined as

$$X_n^{\text{DFT}}[m] = \sum_{k=0}^{N-1} x_{n+k} e^{-\jmath\omega_m k} \tag{1}$$

where $\omega_m = \frac{2\pi m}{N}$. A more theoretically appropriate definition of the DFT is obtained by projecting onto the normalized DFT sinusoids [18], to obtain the normalized DFT (NDFT) of $\mathbf{x}$ given by

$$X_n^{\text{DFT}}[m] = \frac{1}{\sqrt{N}} \sum_{k=0}^{N-1} x_{n+k} e^{-\jmath\omega_m k} \tag{2}$$

Importantly for this work, and contrary to the conventional DFT, only the NDFT provides a rigorous mapping of coordinates from the time-domain to the frequency-domain, that is, it is the NDFT that represents a pure rotation in $\mathbb{C}^N$ which preserves both the orthogonality and the unit-norm properties of the basis sine and cosine functions. The DFT, in contrast, preserves orthogonality, but the norms of the basis functions have the value of $\sqrt{N}$ [18]. The NDFT can thus be rearranged as

$$\begin{aligned} X_n^{\text{DFT}}[m] &= \frac{1}{\sqrt{N}} \sum_{k=0}^{N-1} x_{n+k} e^{-\jmath\omega_m k} \\ &= \frac{1}{\sqrt{N}} \left[\sum_{k=0}^{N-1} x_{n-1+k} e^{-\jmath\omega_m k} + x_{n+N-1} - x_{n-1} \right] e^{\jmath\omega_m} \\ &= \left[X_{n-1}^{\text{DFT}}[m] + \frac{1}{\sqrt{N}} \left(x_{n+N-1} - x_{n-1} \right) \right] e^{\jmath\omega_m} \end{aligned} \tag{3}$$

which is, in effect, a recursive expression for the sliding DFT [19, 20], using normalized DFT sinusoids.

Upon unfolding (3) backward in time, we have

$$\begin{aligned} X_n^{\text{DFT}}[m] &= \left[\left[X_{n-2}^{\text{DFT}}[m] + \frac{1}{\sqrt{N}} \left(x_{n+N-2} - x_{n-2} \right) \right] e^{\jmath\omega_m} \right. \\ &\qquad \left. + \frac{1}{\sqrt{N}} \left(x_{n+N-1} - x_{n-1} \right) \right] e^{\jmath\omega_m} = \cdots \\ &= X_0^{\text{DFT}}[m] e^{\jmath\omega_m n} + \frac{1}{\sqrt{N}} \sum_{k=0}^{n-1} \left(x_{k+N} - x_k \right) e^{-\jmath\omega_m (k-n)} \\ &= \left[X_0^{\text{DFT}}[m] + \frac{1}{\sqrt{N}} \sum_{k=0}^{n-1} \left(x_{k+N} - x_k \right) e^{-\jmath\omega_m k} \right] e^{\jmath\omega_m n} \\ &= \left[\frac{1}{\sqrt{N}} \sum_{k=0}^{N-1} x_{n+k} e^{-\jmath\omega_m (n+k)} \right] e^{\jmath\omega_m n} \\ &= X_n[m] e^{\jmath\omega_m n} \end{aligned} \tag{4}$$

where $X_n[m] = \frac{1}{\sqrt{N}} \sum_{k=0}^{N-1} x_{n+k} e^{-\jmath\omega_m (n+k)}$ is the term which we refer to as the *circularity-preserving DFT* (CPDFT), the operation of which is illustrated in Fig. 1 (left panel).

The conventional DFT computes the phase, $\angle X_n^{\text{DFT}}[m]$, relative to an arbitrary fixed frame of reference. When performing the sliding DFT, a new reference frame is adopted at each time instant n. Such a repeated change in coordinates with each time step increment leads to a rotation in the phase spectrum over time. This follows from the DFT time shift property [21], which states that if

$$\mathbf{x}_n \overset{\mathcal{F}}{\longleftrightarrow} X_n^{\text{DFT}}[m] \quad \text{then} \quad \mathbf{x}_{n+\tau} \overset{\mathcal{F}}{\longleftrightarrow} X_n^{\text{DFT}}[m] e^{\jmath\omega_m \tau} \tag{5}$$

which models the dependence of the phase of the sliding DFT on the time instant n. To account for this dependence, we shall redefine the CPDFT as

$$X_n[m] \triangleq X_n^{\text{DFT}}[m] e^{-\jmath\omega_m n}, \tag{6}$$

so that the phase is projected onto a stationary reference frame, as marked in red in Fig. 1.

Remark 1: Fig. 1 (left panel) shows that the sliding DFT vector rotates counter-clockwise in the complex plane (black dots, phase shifting), while, as desired, the CPDFT maintains a stationary phase (red dot, no rotation).

At each frequency bin, the CPDFT rotates the DFT frame of reference at a rate equal to the frequency at bin index m. This, in turn, shifts the phase spectrum such that the DFT coefficients become stationary over time. This is convenient since time-invariant statistics can then be estimated from the stationary quantities, as the effects of time-varying statistics are eliminated. We can therefore surpass the fictitious circular distributions observed when performing the sliding DFT. In other words, the CPDFT can be thought of as the projection of the complex-valued DFT coefficients onto a stationary reference frame.

Next, we examine the circularity quotient obtained from the sliding DFT [22], that is, $\varrho_n^{\text{DFT}}[m] = E\left\{ {X_n^{\text{DFT}}}^2[m] \right\} / E\left\{ |X_n^{\text{DFT}}[m]|^2 \right\}$:

$$\begin{aligned} \varrho_n^{\text{DFT}}[m] &= \frac{\frac{1}{n} \sum_{k=0}^{n-1} {X_k^{\text{DFT}}}^2[m]}{\frac{1}{n} \sum_{k=0}^{n-1} X_k^{\text{DFT}}[m] {X_k^{\text{DFT}}}^*[m]} \\ &= \frac{\frac{1}{n} \sum_{k=0}^{n-1} X_k^2[m] e^{2\jmath\omega_m k}}{\frac{1}{n} \sum_{k=0}^{n-1} X_k[m] X_k^*[m]} \\ &= \varrho_n[m] \frac{1}{n} \sum_{k=0}^{n-1} e^{2\jmath\omega_m k} \\ &= \varrho_n[m] e^{2\jmath\omega_m \frac{(n-1)}{2}} \mathcal{D}_n(2\omega_m) \end{aligned} \tag{7}$$

where $\varrho_n[m]$ is the circularity quotient of the CPDFT in (6), at time instant n. The last step in (7) relies on the identity

$$\sum_{k=0}^{N-1} e^{\jmath\omega k} = N e^{\jmath\omega \frac{(N-1)}{2}} \frac{\sin\left(\frac{N\omega}{2}\right)}{N \sin\left(\frac{\omega}{2}\right)} = N e^{\jmath\omega \frac{(N-1)}{2}} \mathcal{D}_N(\omega) \tag{8}$$

where $\mathcal{D}_N(\omega) = \frac{\sin\left(\frac{N\omega}{2}\right)}{N \sin\left(\frac{\omega}{2}\right)}$ is the Dirichlet kernel [23], with

$$\lim_{N \to \infty} \mathcal{D}_N(\omega) = 0. \tag{9}$$

It then follows that the longer the sequence use to compute $\varrho_n[m]$, the more circular the DFT, which is obvious from (9), and leads to

$$\lim_{n \to \infty} |\varrho_n[m]| = 0. \tag{10}$$

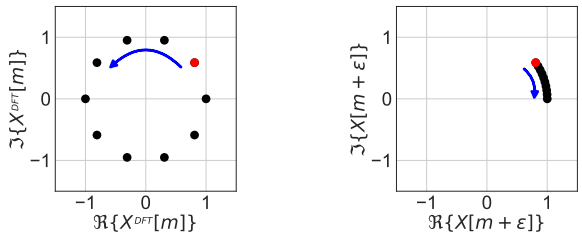

Fig. 1: A scatter diagram of the sliding DFT sequence, $X_m^{\text{DFT}}[m]$, (black dots in left panel), its circularity-preserved version under incoherent sampling, $X_n[m+\epsilon]$, (black dots in right panel), and under coherent sampling, $X_n[m]$, (red dots).

2.2. Spectral whitening and incoherent sampling

The phase spectrum adjustment performed in (6) is only effective when the sampling frequency is an integer multiple of the frequency of interest. In practice, perfect *coherent sampling* is not guaranteed due to either: (i) a finite duration of the data segments or (ii) random frequency fluctuations (intra-wave modulation), which yields further deterministic phase progression and consequently enforces circular complex distributions in time along each frequency bin.

Remark 2: Fig. 1 (right panel) illustrates the slow phase drift associated with incoherent sampling (black dots) of a signal composed of a single sinusoidal component. The mismatch between the sampling frequency, $(m+\epsilon)$, and the fundamental frequency of the sinusoid, m, causes a phase progression of $e^{-\jmath\omega_\epsilon}$ per time step increment, as proven analytically next.

Consider a signal $\mathbf{x}_n = [x_n, ..., x_{n+N-1}]^T \in \mathbb{R}^N$ composed of a sinusoidal component at a frequency bin m, and assume that the signal is sampled at a frequency $(m+\epsilon)$, that is, with a small frequency offset ϵ. From the frequency translation property

$$\mathbf{x}_n \overset{\mathcal{F}}{\longleftrightarrow} X_n^{\text{DFT}}[m] \quad \text{then} \quad \mathbf{x}_n e^{-\jmath\omega_\epsilon n} \overset{\mathcal{F}}{\longleftrightarrow} X_n^{\text{DFT}}[m+\epsilon] \tag{11}$$

and we therefore have

$$X_n^{\text{DFT}}[m+\epsilon] = \sum_{k=0}^{N-1} \left(x_{n+k} e^{-\jmath\omega_\epsilon n}\right) e^{-\jmath\omega_m k} = X_n[m] e^{-\jmath\omega_\epsilon n} \tag{12}$$

that is, $X_n[m]$ is rotated by $-\omega_\epsilon$ with each time step increment.

Remark 3: Under incoherent sampling, the sampling frequency mismatch, $-\epsilon$, will yield a slow rotation in the sliding DFT, at a speed of ω_ϵ in time. This causes the sliding DFT to exhibit less noncircular distribution; observe that the more samples over which the sample circularity quotient is computed in (7), the more circular the distribution of $X_n[m]$. In other words, for a finite number of samples, the degree of noncircularity of an incoherently sampled signal will be under-estimated.

To derive a closed-form expression for the sample circularity of $X_n[m]$ under incoherent sampling [15], from (7) we have

$$\begin{aligned}
\varrho_n[m+\epsilon] &= \frac{\frac{1}{n}\sum_{k=0}^{n-1} X_k^2[m+\epsilon]}{\frac{1}{n}\sum_{k=0}^{n-1} X_k[m+\epsilon] X_k^*[m+\epsilon]} \\
&= \frac{\frac{1}{n}\sum_{k=0}^{n-1} X_k^2[m] e^{-2\jmath\omega_\epsilon k}}{\frac{1}{n}\sum_{k=0}^{n-1} X_k[m] X_k^*[m]} \\
&= \varrho_n[m] \frac{1}{n} \sum_{k=0}^{n-1} e^{-2\jmath\omega_\epsilon k} \\
&= \varrho_n[m] e^{-2\jmath\omega_\epsilon \frac{(n-1)}{2}} \mathcal{D}_n(2\omega_\epsilon).
\end{aligned} \tag{13}$$

Using properties of Dirichlet's kernel [23], the following holds

$$\lim_{\epsilon\to 0} \varrho_n[m+\epsilon] = \varrho_n[m], \quad \lim_{\epsilon\to\pm\infty} |\varrho_n[m+\epsilon]| = 0 \tag{14}$$

Remark 4: The spectral circularity quotient $\varrho_n[m+\epsilon]$ is dependent on the sampling frequency mismatch ϵ.

We next propose a method to remove the effects of the incoherent sampling by tracking the expected frequency mismatch. From (12), the effects of incoherent sampling can be mitigated by an additional phase adjustment. In other words, to cancel out the effect of incoherent sampling, the circularity-preserved phase spectrum, $\angle X_n[m]$, must be shifted by the expected phase progression from the frequency mismatch at each frequency bin, ϕ_m, between the consecutive CPDFT values, that is,

$$\begin{aligned}
\phi_m &= E\left\{\angle X_n[m+\epsilon] - \angle X_{n-1}[m+\epsilon]\right\} \\
&= E\left\{-\omega_\epsilon n + \omega_\epsilon(n-1)\right\} \\
&= E\left\{-\omega_\epsilon\right\}
\end{aligned} \tag{15}$$

The overall adjustment to the conventional DFT, when accounting for incoherent sampling, therefore becomes

$$\begin{aligned}
X_n[m] &= \frac{1}{\sqrt{N}} \sum_{k=0}^{N-1} x_{n+k} e^{-\jmath[\omega_m(n+k)+\phi_m n]} \\
&= X_n[m+\epsilon] e^{-\jmath\phi_m n} \\
&= X_n^{\text{DFT}}[m+\epsilon] e^{-\jmath[\omega_m+\phi_m]n}
\end{aligned} \tag{16}$$

Remark 5: The behaviour of the phase mismatch, ϕ_m in (15), depends on whether the input signal, $\mathbf{x}_n$, is a deterministic or a stochastic process.

2.2.1. *Behaviour of ϕ_m for a deterministic input*

If at the mth frequency bin the sampling frequency is an integer multiple of m (coherent sampling), then the expected phase mismatch between the consecutive $X_n[m]$ and $X_{n-1}[m]$ will equal 0, that is

$$\begin{aligned}
\phi_m &= E\left\{\angle X_n[m+\epsilon] - \angle X_{n-1}[m+\epsilon]\right\} \\
&= E\left\{\angle X_n[m] - \angle X_{n-1}[m]\right\} = 0
\end{aligned} \tag{17}$$

This holds even if the signal is contaminated with noise, owing to the expectation operator $E\{\cdot\}$. Intuition into why the determinism within $X_n[m]$ will manifest itself as a noncircular distribution is in that the distribution of $X_n[m]$ will lie on a line of constant phase, as shown in Fig. 1 (red dot), which in turn means that its distribution will inherently be rotation-variant, and thus noncircular.

Under incoherent sampling, the expected phase mismatch between the consecutive $X_n[m+\epsilon]$ and $X_{n-1}[m+\epsilon]$ will become approximately constant, that is,

$$\phi_m = E\left\{\angle X_n[m+\epsilon] - \angle X_{n-1}[m+\epsilon]\right\} = -\omega_\epsilon, \tag{18}$$

where ω_ϵ is the constant phase mismatch between the sampling frequency $(m+\epsilon)$ and the neighbouring deterministic "interharmonic" true frequency m. Condition (18) also holds true in the presence of noise. Similarly, $X_n[m+\epsilon]$ will lie on a line of constant phase, which means that the distribution will inherently be rotation-dependent, and thus noncircular.

2.2.2. *Behaviour of ϕ_m for a stochastic input*

Regardless of the sampling coherence at the mth frequency bin, if $X_n[m]$ is complex-Gaussian distributed then the expected phase mismatch between the consecutive $X_n[m+\epsilon]$ and $X_{n-1}[m+\epsilon]$ will be uniformly distributed in the dense set $[0, 2\pi)$, that is

$$\phi_n = E\left\{\angle X_n[m+\epsilon] - \angle X_{n-1}[m+\epsilon]\right\} \in [0, 2\pi). \tag{19}$$

This provides intuition into why a uniformly distributed $X_n^{\text{DFT}}[m]$ will remain uniformly distributed upon phase-rotating to $X_n[m]$. The distribution of $\angle X_n[m]$ will also be uniform within the dense set $[0, 2\pi)$, so that the distribution of $X_n[m]$ will inherently be rotation-invariant, and thus circular. This property inherits from the definition of a circular distribution, that is, that the distribution of $X_n^{\text{DFT}}[m]$ is equivalent to the distribution of $X_n^{\text{DFT}}[m]e^{\jmath\theta}\ \forall\theta$ [24].

To track the expected phase mismatch at a time instant n, $\phi_{m,n}$, for simplicity and robustness we can employ a moving-average of the phase mismatch

$$\phi_{m,n} = \frac{1}{N}\sum_{l=0}^{L-1}\Big[\angle X_{n-l}[m] - \angle X_{n-1-l}[m]\Big] \tag{20}$$

More sophisticated procedures employ the Kalman filter or recursive least squares [25, 26, 27, 28, 29, 30], but require tuning of additional parameters.

Remark 6: Fig. 1 (right panel) illustrates that under incoherent sampling the sliding DFT vector rotates clockwise (black dots), while, as desired, the CPDFT maintains a stationary phase (red dot).

3. ADAPTIVE ESTIMATION OF THE PANORAMA

There is an intricate link between the circularity quotient and the frequency-domain Wiener solution [31], given by

$$w[m] = \frac{E\left\{D_n^*[m]X_n[m]\right\}}{E\left\{|X_n[m]|^2\right\}} \tag{21}$$

for an input signal, $\mathbf{x}_n \in \mathbb{R}^N$ with $\mathbf{x}_n \overset{\mathcal{F}}{\longleftrightarrow} X_n[m]$, and a desired signal $\mathbf{d}_n \in \mathbb{R}^N$ with $\mathbf{d}_n \overset{\mathcal{F}}{\longleftrightarrow} D_n[m]$. We next provide a novel insight through the circularity quotient of a complex-valued random variable $x \in \mathbb{C}$, defined as $\varrho = E\left\{x^2\right\}/E\left\{|x|^2\right\}$ [22].

Since the Wiener filter is computationally expensive and cannot operate in real time, the recent work in [31] demonstrates that a complex least mean-square (CLMS) algorithm can be used to recursively track the circularity quotient of complex-valued signal. We next utilise the CLMS to estimate the panorama from the CPDFT, $P_n[m] = E\left\{X_n^2[m]\right\}$, and in this way bypass the key stumbling block in the practical applications of the panorama - the requirement for ensemble averages.

Consider using a zero-mean random variable $z \in \mathbb{C}$ to estimate the zero-mean random variable $d \in \mathbb{C}$, in the form $d = w^* z$, where $w \in \mathbb{C}$ is a weight coefficient. The minimum mean square error (MMSE) estimator seeks the optimal value of w [31] by minimizing the cost function $J_{\text{MSE}} = E\{ee^*\}$, where $e = d - w^* z$ is the estimation error. The solution sets $\frac{\partial J_{\text{MSE}}}{\partial w^*} = 0$ and solves for w. For convenience, we utilize the $\mathbb{CR}$ (or Wirtinger) derivative chain rule [32, 4] to simplify $\frac{\partial J_{\text{MSE}}}{\partial w^*}$ to $\frac{\partial J_{\text{MSE}}}{\partial w^*} = \frac{\partial J_{\text{MSE}}}{\partial e}\frac{\partial e}{\partial w^*} + \frac{\partial J_{\text{MSE}}}{\partial e^*}\frac{\partial e^*}{\partial w^*} = 0$. Upon inserting $\frac{\partial e}{\partial w^*} = -z$, $\frac{\partial e^*}{\partial w^*} = 0$ and $\frac{\partial J_{\text{MSE}}}{\partial e} = e^*$ we have

$$\frac{\partial J_{\text{MSE}}}{\partial w^*} = -E\left\{e^* x\right\} = -E\{d^* z - wzz^*\} = 0. \tag{22}$$

Therefore, for the optimal circularity tracker

$$w_{\text{opt}} = \frac{E\{d^* z\}}{E\{zz^*\}}. \tag{23}$$

Finally, the gradient descent update, $w_{n+1} = w_n - \mu\frac{\partial J_{\text{MSE}}}{\partial w^*}$, gives

$$w_{n+1} = w_n + \mu e^* x. \tag{24}$$

Remark 7: Real time spectral circularity tracking can be performed based on (23) with the choice of parameters, $d^* = z = X_n[m]$, to yield

$$w_{\text{opt}} = \frac{E\{X_n^2[m]\}}{E\{X_n[m]X_n^*[m]\}} = \frac{P_n[m]}{R_n[m]} = \varrho_n[m], \tag{25}$$

which is the spectral circularity of $\mathbf{x}_n$ at a frequency bin m.

Remark 8: From (25), the panorama can be computed from CPDFT in real time, based on the single-realisation of the input signal as

$$P_n[m] = E\left\{X_n^2[m]\right\}. \tag{26}$$

Remark 9: Unlike the existing ensemble or block-based estimators of the panorama, based on (25) the panorama can be estimated from the standard power spectrum and spectral circularity for a single streaming realisation as $P_n[m] = \varrho_n[m]R_n[m]$.

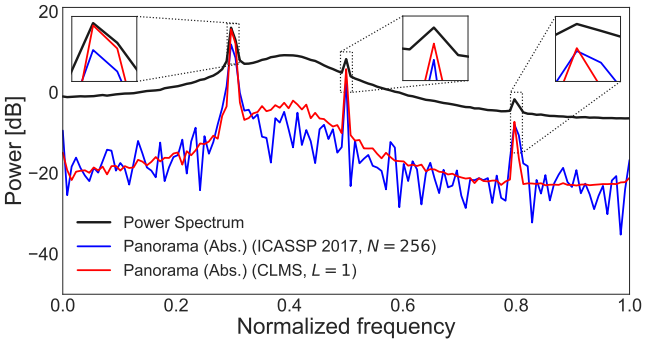

Fig. 2: The panorama estimators, block and recursive.

4. SIMULATIONS

The performance of the proposed spectral circularity estimator is illustrated through an example, which for continuity is identical to that from [5, 7], where the signal of interest if given by

$$\begin{aligned} x_n = &\cos\left(0.15(2\pi n) - \frac{\pi}{6}\right) + 0.25\cos\left(0.25(2\pi n) + \frac{\pi}{3}\right) \\ &+ 0.1\cos\left(0.4(2\pi n) + \frac{\pi}{8}\right) + \eta_n, \end{aligned} \tag{27}$$

and η_n is a zero-mean Gaussian random process generated by filtering a zero-mean uncorrelated Gaussian random process with a digital filter with the system function given by

$$H(z) = \frac{1}{1 - 1.6\cos(2\pi 0.2)z^{-1} + 0.64z^{-2}}. \tag{28}$$

A single 100,000-sample realization was generated, and the sliding DFT of x_n was estimated using (16), with a window of $N = 256$ samples in length. Fig. 2 compares the performance of the proposed panorama estimator against the power spectrum and the recently introduced time-average based panorama estimator [7].

For a fair comparison, the method from [7] was employed using a window length of size $N = 256$. The CLMS-based panorama estimator had a filter length of $L = 1$, and the moving-average window used to estimate the phase mismatch from (20), ϕ_m, was $N = 256$ samples in length.

While the single-realisation panorama estimator in [7] is block-based, the proposed CLMS-based estimator operates in a real-time fashion and achieved a very similar performance to the existing method, offering 20 dB noise suppression. An additional significant advantage is that in this way, it makes it possible to estimate the panorama adaptively, with minimal computational complexity, making it suitable for the use with real-time and streaming data. The proposed estimator also allows for causal processing as the estimate at a time instant n depends on the past and current inputs only, in contrast to the method in [7] which employs a non-causal approach.

5. CONCLUSIONS

We have introduced a procedure for preserving the spectral circularity of the sliding DFT of noisy real-valued signals in real-time, for the critical cases of incoherent sampling and short data lengths. In conjunction with Wiener filtering and its recursive estimation, this has served as a basis to estimate both the spectral circularity and the panorama, from a single realisation of a signal. Numerical evaluations have demonstrated the usefulness of the proposed technique for both online spectral estimation and noise suppression. The distinguishing advantage of the proposed framework has been shown to arise from the additional degree of freedom in the analysis, stemming from the complex-valued nature of the panorama (*cf.* standard real-valued power spectrum).

6. REFERENCES

[1] D. P. Mandic, S. Javidi, G. Souretis, and V. S. L. Goh, "Why a Complex Valued Solution for a Real Domain Problem," *In Proceedings of the IEEE Workshop on Machine Learning for Signal Processing*, pp. 384–389, 2007.

[2] S. Wisdom, L. Atlas, J. Pitton, and G. Okopal, "Benefits of Noncircular Statistics for Nonstationary Signals," *In Proceedings of the 50th Asilomar Conference on Signals, Systems and Computers*, pp. 554–558, 2016.

[3] F. D. Naseer and J. L. Massey, "Proper Complex Random Processes with Applications to Information Theory," *IEEE Transactions on Information Theory*, vol. 39, no. 4, pp. 1293–1302, 1993.

[4] D. P. Mandic and V. S. L. Goh, *Complex Valued Nonlinear Adaptive Filters: Noncircularity, Widely Linear and Neural Models*. New York: Wiley, 2009.

[5] S. C. Douglas and D. P. Mandic, "Autoconvolution and Panorama: Augmenting Second-Order Signal Analysis," *In Proceedings of the IEEE International Conference on Acoustic, Speech and Signal Processing (ICASSP)*, pp. 384–388, 2014.

[6] B. Picinbono, "On Circularity," *IEEE Transactions on Signal Processing*, vol. 42, no. 12, pp. 3473–3482, 1994.

[7] S. C. Douglas and D. P. Mandic, "Single-Channel Wiener Filtering of Deterministic Signals in Stochastic Noise using the Panorama," *In Proceedings of the IEEE International Conference on Acoustic, Speech and Signal Processing (ICASSP)*, pp. 1182–1186, 2017.

[8] P. J. Schreier and L. L. Scharf, "Stochastic Time-Frequency Analysis Using the Analytic Signal: Why the Complementary Distribution Matters," *IEEE Transactions on Signal Processing*, vol. 51, no. 12, pp. 3071–3079, 2003.

[9] B. Rivet, L. Girin, and C. Jutten, "Log-Rayleigh Distribution: A Simple and Efficient Statistical Representation of Log-Spectral Coefficients," *IEEE Transactions on Audio, Speech and Language Processing*, vol. 15, no. 3, pp. 796–802, 2007.

[10] P. Clark, "Coherent Demodulation of Nonstationary Random Processes," Ph.D. Dissertation, University of Washington, 2012.

[11] P. Clark, I. Kirsteins, and L. Atlas, "Existence and Estimation of Impropriety in Real Rhythmic Signals," *in Proceedings of IEEE International Conference on Acoustics, Speech and Signal Processing (ICASSP)*, vol. 108, pp. 3713–3716, 2012.

[12] S. Wisdom, L. Atlas, and J. Pitton, "Extending Coherence Time for Analysis of Modulated Random Processes," *IEEE International Conference on Acoustics, Speech and Signal Processing (ICASSP)*, pp. 340–344, 2014.

[13] S. Wisdom, G. Okopal, L. Atlas, and J. Pitton, "Voice Activity Detection Using Subband Noncircularity," *In Proceedings of the IEEE International Conference on Acoustics, Speech and Signal Processing (ICASSP)*, pp. 4505–4509, 2015.

[14] G. Okopal, S. Wisdom, and L. Atlas, "Estimating the Noncircularity of Latent Components within Complex-Valued Subband Mixtures with Applications to Speech Processing," *In Proceedings of the Asilomar Conference on Signals, Systems, and Computers*, pp. 1405–1409, 2014.

[15] ——, "Speech Analysis With the Strong Uncorrelating Transform," *IEEE/ACM Transactions on Audio, Speech, and Language Processing*, vol. 23, no. 11, pp. 1858–1868, 2015.

[16] E. Ollila, "On the Circularity of a Complex Random Variable," *IEEE Signal Processing Letters*, vol. 15, pp. 841–844, 2008.

[17] S. Wisdom, L. Atlas, and J. Pitton, "On Spectral Noncircularity of Natural Signals," *In Proceedings of the Sensor Array and Multichannel Signal Processing Workshop (SAM)*, pp. 1–5, 2016.

[18] J. O. Smith, *Mathematics of the Discrete Fourier Transform (DFT) with Audio Applications*. Stanford: W3K Publishing, 2007.

[19] E. Jacobsen and R. Lyons, "The Sliding DFT," *IEEE Signal Processing Magazine*, vol. 20, no. 2, pp. 74–80, 2003.

[20] ——, "An Update to The Sliding DFT," *IEEE Signal Processing Magazine*, vol. 21, no. 1, pp. 110–111, 2004.

[21] T. Springer, "Sliding FFT Computes Frequency Spectra in Real Time," *EDN Magazine*, pp. 161–170, 1988.

[22] J. Eriksson, E. Ollila, and V. Koivunen, "Essential Statistics and Tools for Complex Random Variables," *IEEE Transactions on Signal Processing*, vol. 58, no. 10, pp. 5400–5408, 2010.

[23] D. Percival and A. Walden, *Spectral Analysis for Physical Applications*. Cambridge: Cambridge University Press, 1993.

[24] P. J. Schreier and L. L. Scharf, *Statistical Signal Processing of Complex-Valued Data: The Theory of Improper and Noncircular Signals*. Cambridge University Press, 2010.

[25] A. G. Phadke and M. G. Adamiak, "A New Measurement Technique for Tracking Voltage Phasors, Local System Frequency, and Rate of Change of Frequency," *IEEE Transactions on Power Apparatus and Systems*, vol. PAS-102, no. 5, pp. 1025–1038, 1983.

[26] J. Z. Yang and C. W. Liu, "A Precise Calculation of Power System Frequency," *IEEE Transactions on Power Delivery*, vol. 16, no. 2, pp. 361–366, 2001.

[27] M. Wang and Y. Sun, "A Practical Method to Improve Phasor and Power Measurement Accuracy of DFT Algorithm," *IEEE Transactions on Power Delivery*, vol. 21, no. 3, pp. 1054–1062, 2006.

[28] B. Borkowski and A. Bien, "A Practical, Precise Method for Frequency Tracking and Phasor Estimation," *IEEE Transactions on Power Delivery*, vol. 24, no. 3, pp. 1004–1013, 2009.

[29] J. R. Carvalho, C. A. Duque, M. A. A. Lima, D. V. Coury, and P. F. Ribeiro, "A Novel DFT-Based Method for Spectral Analysis under Time-Varying Frequency Conditions," *Electric Power Systems Research*, vol. 108, pp. 74–81, 2014.

[30] X. Yili, Y. He, K. Wang, W. Pei, Z. Blazic, and D. P. Mandic, "A Complex Least Squares Enhanced Smart DFT Technique for Power System Frequency Estimation," *IEEE Transactions on Power Delivery*, vol. 32, no. 3, pp. 1270–1278, 2017.

[31] S. Kanna, S. C. Douglas, and D. P. Mandic, "A Real Time Tracker of Complex Circularity," *In Proceedings of the IEEE 8th Sensor Array and Multichannel Signal Processing Workshop (SAM)*, pp. 129–132, 2014.

[32] K. Kreutz-Delgado, "The Complex Gradient Operator and the CR-Calculus," arXiv:0906.4835v1 [math.OC]. [Online]. Access: https://arxiv.org/abs/0906.4835, 2009.